Nucleotides and transported substrates modulate different steps of the ATPase catalytic cycle of MRP1 multidrug transporter

András KERN*, Zsófia SZENTPÉTERY*, Károly LILIOM*, Éva BAKOS*, Balázs SARKADI† and András VÁRADI*[1]

*Institute of Enzymology, Hungarian Academy of Sciences, 29 Karolina út, 1113 Budapest, Hungary, and †National Medical Center, Institute of Haematology and Immunology, Membrane Research Group, Hungarian Academy of Sciences, 64 Diószegi utca, 1113 Budapest, Hungary

The human ABC (ATP-binding cassette) transporter MRP1 (human multidrug-resistance-associated protein 1; ABCC1) is involved in the cellular extrusion of conjugated metabolites and causes multidrug resistance in tumour cells. The transport of substrate molecules by ABC proteins is energized by ATP hydrolysis, performed by two co-operating ABC units. Orthovanadate (Vi), a non-covalent inhibitor of the ABC ATPases, was found to catalyse a photo-oxidative cleavage of various ATP-binding proteins. In the present study, we have identified three Vi-cleavage sites within MRP1, and found that the cleavage reactions were variably modulated by the presence of nucleotides and by transported substrates. We concluded that Vi cleavage of MRP1 at Site I detects conformational changes due to the binding of MgATP. In contrast, Site II could be identified as part of the substrate-modulated catalytic cycle, probably containing an MRP1 · MgADP · Vi transition-state-like complex. Cleavage at Site III was modulated by both the binding and hydrolysis of MgATP, in a biphasic pattern, which was also affected by the presence of transported substrates. We detected two different allosteric effects and found that they control two consecutive steps of the MRP1 ATPase catalytic cycle. Nucleotide binding to the low-affinity site accelerated the formation of the pre-hydrolytic intermediate in the other catalytic centre. Interaction of the transporter with its transported substrates stimulated a later reaction of the hydrolytic cycle, the formation of the post-hydrolytic intermediate, which could be detected in both catalytic sites by the experimental strategy used.

Key words: ATP-binding cassette transporter (ABC transporter), ATPase catalytic cycle, multidrug-resistance-associated protein 1 (MRP1), pre- and post-hydrolytic intermediate, transition state, vanadate cleavage.

INTRODUCTION

A specific feature of the orthovanadate anion, VO_4^{3-} (Vi), is that it can catalyse photo-oxidation of the polypeptide chains upon UV irradiation. The Vi-catalysed photo-oxidation causes a cleavage of the polypeptide chain in the vicinity of the site where Vi binds to the protein. Indeed, in myosin, a polypeptide cleavage was observed at the glycine-rich motif (also called a Walker A motif), which is known to be involved in interactions with the phosphate moiety of the nucleotide [1]. The mechanism of the reaction, involving the oxidation of the hydroxymethyl side-chains of a serine residue to a serine aldehyde via light-catalysed reduction of V^V (vanadate) to V^{IV} (vanadyl), and a subsequent backbone cleavage at this serine residue, has been elucidated [2].

On the other hand, Vi is an effective non-covalent inhibitor of several ATP-hydrolysing enzymes. Comparing the three-dimensional structure of the MgATP-bound form of the myosin motor domain to that of the MgADP · Vi inhibitor complex revealed that Vi occupies the position of the terminal phosphate in the catalytic complex, accommodating a trigonal bipyramidal coordination [3]. The enzyme · MgADP · Vi complex is supposed to model one of the high-energy transition states of the catalytic cycle of Vi-sensitive ATPases. Other anions with similar geometry and charges (e.g. AlF_4 or BeF_x) are also capable of inhibiting the same class of ATPases, arresting the enzymes in similar, although not necessarily identical, inhibitory complex forms [4]. Therefore these anions are widely used in studying the mechanism of ATP hydrolysis. The complex is usually visualized by covalent photoaffinity labelling, using 8-azido-[α-^{32}P]ATP.

Multidrug resistance is a major obstacle in the efficient chemotherapy of human malignancies. The emergence of this phenomenon is frequently associated with the overexpression of special ABC (ATP-binding cassette) transporter proteins, such as MDR1 (multidrug resistance 1; ABCB1), MRP1 (human multidrug-resistance protein 1; ABCC1) and BCRP (breast-cancer-resistance protein; ABCG2) in tumour cells. ABC transporters are composed of TMDs (transmembrane domains) and ABC domains. In MRP1, the sites that interact with the drug substrates are harboured within the TMDs and in the L0 and L1 intracellular linker segments [5–9], and ATP hydrolysis, as in other ABC proteins, is coupled to transmembrane substrate movement. Vi, as well as AlF_4 or BeF_x, is an effective inhibitor of these types of transporters. A unique feature of ABC proteins is that they are composed of two homologous ABC units, where ATP binding and hydrolysis occur. A tight functional co-operativity between the two ABC units is a prerequisite of the activity of the ABC ATPases. A general model, based on the X-ray crystallographic analysis of the ABC–ABC dimer of a bacterial ABC ATPase Rad50cd, suggests that the structural basis of the co-operativity is that the two ABC units form two composite active sites in a head-to-tail configuration [10]. Elements of both ABC units participate in the composition of the two active sites. Similar arrangement of the ABC ATPase catalytic sites has been found recently in the BtuCD ABC transporter of *Escherichia coli* [11].

Formation of an enzyme · MgADP · Vi complex (occluded nucleotide state, or nucleotide trapping) in various ABC ATPases was demonstrated and utilized for mechanistic studies [15–18]. In the case of MDR1, azido-ATP photolabelling experiments

Abbreviations used: ABC, ATP-binding cassette; HAS, high-affinity site; LAS, low-affinity site; LTC_4, leukotriene C_4; MDR1, multidrug resistance 1 (ABCB1); MgAMP-PCP, magnesium adenosine 5′-(β,γ-methylene)triphosphate; MRP1, human multidrug-resistance-associated protein 1 (ABCC1); ΔMRP1, MRP1 with a deletion of residues 1–280; Sf9 cells, *Spodoptera frugiperda* ovarian cells; TMD, transmembrane domain; Vi, orthovanadate.

[1] To whom correspondence should be addressed (e-mail varadi@enzim.hu).

revealed that both ABC units play essential roles in ATP hydrolysis [19,20]. The examination of the Vi-catalysed photo-oxidative cleavage in MDR1 provided strong evidence for an alternating ATP hydrolysis by two equivalent catalytic sites [21].

In the case of MRP1, the catalytic/transport mechanism has been the subject of several studies [22–28]. Three independent studies found major differences in the catalytic properties of the two ABC units. Photolabelling by azido-ATP, and following the formation of an enzyme · Mg(azido)ADP · Vi complex led to the postulation that the two ABC units fulfil unequal roles in the activity of MRP1 [22–24]. It was suggested that one of the nucleotide-binding sites in MRP1 is dominant in the cleavage cycle, while the site in the other ABC unit can only perform nucleotide binding [22–25,27,28].

In the present study, we used the Vi-induced photocleavage reaction for characterizing the interactions of MRP1 with nucleotides and transported substrates. We could detect two different allosteric effects during the MRP1 ATPase cycle, and we found that they control two different steps of the catalysis. Nucleotide-binding to one of the sites induced a positive allosteric effect on the formation of a pre-hydrolytic intermediate complex in the other site, while interaction with the transported substrates stimulates the formation of the post-hydrolytic intermediates. In addition, we found post-hydrolytic complex formation in both catalytic sites, which means that both sites are catalytically active during ATP hydrolysis and are under a transported substrate-mediated allosteric control.

MATERIALS AND METHODS

Protein expression and assay of ATPase activity

Expression of MRP1 and ΔMRP1 (MRP1 with a deletion of residues 1–280) in Sf9 (*Spodoptera frugiperda*) insect cells, membrane preparation and determination of Vi-sensitive ATPase activity were performed as described in our previous publications [29–32].

Vi-induced photo-oxidative cleavage

Stock solutions of sodium orthovanadate were prepared as described in [33]. The A_{265} of the solution was determined, and the Vi concentration was calculated using the molar absorption coefficient of 2925 $M^{-1} \cdot cm^{-1}$.

Samples containing the isolated Sf9 cell membranes (20 mg/ml) expressing MRP1 (or ΔMRP1) were pre-incubated at 37 °C for 5 min in the presence of 0.8 mM sodium orthovanadate and in the presence or absence of transported substrates in the reaction buffer (50 mM Mops/Tris, pH 7.4, 50 mM KCl and 10 mM $MgCl_2$). Various concentrations of MgATP {or MgAMP-PCP [magnesium adenosine 5′-(β,γ-methylene)triphosphate]} were subsequently added to the samples (as indicated in the Figures) at a final volume of 40 μl, and the tubes were incubated for an additional 5 min at 37 °C for N-terminal cleavage (to generate the f95 and f85 fragments; see below) and for 20 min at 37 °C for C-terminal cleavage (to generate a f25 fragment; see below). After incubation, the reaction mixture was immediately transferred on to ice. In reactions where photoactivation was induced by UV light, the samples were transferred on to ice and placed under a 265-nm UV lamp at a distance of 5 cm. The samples were irradiated for 10 min for N-terminal cleavage and 2 min for C-terminal cleavage. After irradiation, the 10 μl sample buffer [50 mM Tris/phosphate, pH 6.8, 2 % (w/v) SDS, 2 % (w/v) 2-mercaptoethanol, 2 mM EDTA, 20 % (v/v) glycerol and 0.02 % (w/v) Bromophenol Blue] was added to the reaction mixture and the samples were subjected to SDS/PAGE and immunoblot analysis.

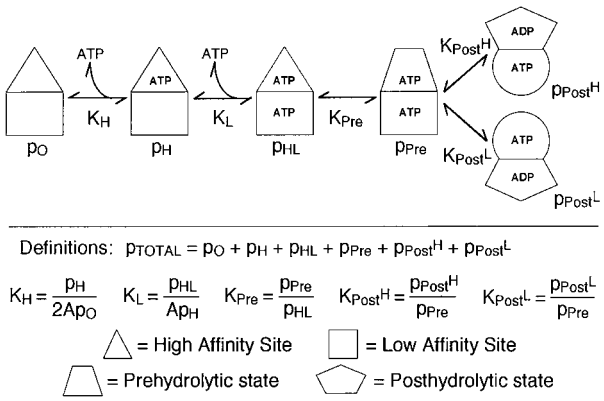

Scheme 1 Equilibrium model of MRP1 ATPase hydrolytic cycle

SDS/PAGE, immunoblot and densitometry analysis, and 8-azido-ATP-binding

SDS/PAGE was performed using 7.5 % or 15 % (w/v) polyacrylamide gels, followed by immunoblotting as described in [29]. Detection of human MRP1 with M6 mouse anti-MRP monoclonal antibodies (diluted 1:10 000) were performed as described in [34]. Secondary antibodies were obtained from Jackson ImmunoResearch (horseradish-peroxidase-conjugated donkey anti-mouse IgG; diluted 1:10 000). Immunoreactive bands were visualized by enhanced chemiluminescence (ECL®; Amersham Biosciences). The bands were quantified by densitometry on ChemiDoc XRS (Bio-Rad) using the Quantity One (Bio-Rad) software. Calibration curves were established to determine the linear range of the density signal for each bands studied, and data were analysed by the KaleidaGraph software package (Synergy Software, Reading, PA, U.S.A.). 8-azido-ATP-binding experiments were performed as described in [34].

Mathematical modelling of the ATPase hydrolytic cycle

We have developed a mathematical model to describe those conformational intermediates, occurring during ATP-hydrolysis by MRP1, that can be distinguished using the Vi-induced photo-oxidative cleavage reaction (see Scheme 1). The model consists of ATP binding to the high-affinity site (HAS) first ($p_O \rightarrow p_H$ transition), then to the low-affinity site (LAS) ($p_H \rightarrow p_{HL}$ transition), followed by a conformational change at the HAS yielding the pre-hydrolytic intermediate ($p_{HL} \rightarrow p_{Pre}$ transition). We supposed that, in the presence of Vi, MRP1 can reach two different states from this pre-hydrolytic conformation, one where the HAS is in the post-hydrolytic state ($p_{Pre} \rightarrow p_{Post}{}^H$ transition) and another where the LAS is in the post-hydrolytic state ($p_{Pre} \rightarrow p_{Post}{}^L$ transition) (see the Discussion). At equilibrium, this set of reactions (Scheme 1) can be described with the following set of equations (eqns 1a–1e):

$$K_H = p_H/(2Ap_O) \quad (1a)$$

$$K_L = p_{HL}/(Ap_H) \quad (1b)$$

$$K_{Pre} = p_{Pre}/p_{HL} \quad (1c)$$

$$K_{Post}{}^H = p_{Post}{}^H/p_{Pre} \quad (1d)$$

$$K_{Post}{}^L = p_{Post}{}^L/p_{Pre} \quad (1e)$$

where A denotes the equilibrium concentration of free ATP; p_O, p_H, p_{HL}, p_{Pre}, $p_{Post}{}^H$ and $p_{Post}{}^L$ denote the equilibrium concentrations of the different MRP1 conformational states that occur during the hydrolytic cycle; K_H and K_L are the intrinsic association constants for ATP binding to the HAS and LAS respectively; and K_{Pre}, $K_{Post}{}^H$ and $K_{Post}{}^L$ are the isomerization constants for the $p_{HL} \rightarrow p_{Pre}$, $p_{Pre} \rightarrow p_{Post}{}^H$ and $p_{Pre} \rightarrow p_{Post}{}^L$ transitions respectively.

Also, the mass-conversation law for the different conformers of MRP1 is defined by eqn (2):

$$p_O + p_H + p_{HL} + p_{Pre} + p_{Post}{}^H + p_{Post}{}^L = p_{TOTAL} \quad (2)$$

where p_{TOTAL} denotes the total concentration of MRP1 present. The normalized concentrations of the three fragments, f95, f85 and f25 (fragments of 95, 85 and 25 kDa respectively), obtained by Vi cleavage at Site I, II and III respectively (see the Results section), relative to the total concentration of MRP1, can be calculated as follows.

At Site I, Vi can only cleave those MRP1 conformers where the LAS is not occupied by ATP. The presence of nucleotide decreases the amount of the 95 kDa cleavage product in a concentration-dependent manner (see the Results section), so we analysed the disappearance of f95. Consequently, the normalized concentration of f95 is proportional to those conformational states where the LAS is occupied by ATP, that is $p_{HL} + p_{Pre}$. At Site II, those protein molecules can be cleaved where the LAS is in the post-hydrolytic complex conformation, so the appearance of f85 is proportional to $p_{Post}{}^L$. At Site III, the Vi-accessible conformers are those where the HAS is occupied by ATP, so the appearance of f25 is proportional to $p_H + p_{HL}$. These assumptions yield, with simple algebraic rearrangements of eqns (1a–1e) and eqn (2), the following equations for the three fragments:

$$f95 \sim \frac{p_{HL} + p_{Pre}}{p_{TOTAL}} = \frac{2A^2K_HK_L(1 + K_{Pre})}{1 + 2AK_H\{1 + AK_L[1 + K_{Pre}(1 + K_{Post}{}^H + K_{Post}{}^L)]\}} \quad (3)$$

$$f85 \sim \frac{p_{Post}{}^L}{p_{TOTAL}} = \frac{2A^2K_HK_LK_{Pre}K_{Post}{}^L}{1 + 2AK_H\{1 + AK_L[1 + K_{Pre}(1 + K_{Post}{}^H + K_{Post}{}^L)]\}} \quad (4)$$

$$f25 \sim \frac{p_H + p_{HL}}{p_{TOTAL}} = \frac{2AK_H(1 + AK_L)}{1 + 2AK_H\{1 + AK_L[1 + K_{Pre}(1 + K_{Post}{}^H + K_{Post}{}^L)]\}} \quad (5)$$

These formulae (eqn 3–5) were used in a global fitting procedure (see Discussion) in order to obtain estimates for the model parameters (the intrinsic association constants K_H and K_L as well as the isomerization constants K_{Pre}, $K_{Post}{}^H$ and $K_{Post}{}^L$), using the non-linear curve-fitting module of KaleidaGraph.

RESULTS

Human MRP1 and ΔMRP1 were expressed in Sf9 insect cells, and isolated cell membranes were used for the photo-oxidative cleavage reactions. The expressed MRP1 protein in isolated membranes was fully active, as demonstrated by assaying its specific drug-stimulated, Vi-sensitive ATPase activity ($V_{max} = 19.8 \pm 4.8$ nmol of P_i/min per mg of protein in the presence of 5 mM *N*-ethylmaleimide S-glutathione), while ΔMRP1 showed no measurable ATPase activity.

The membrane samples containing human MRP1 or ΔMRP1 were subjected to photo-oxidative cleavage, as described in the Materials and methods section, and the cleavage products were analysed by SDS/PAGE and subsequent immunoblotting. In the experiments presented below, a monoclonal antibody, M6, recognizing an extreme C-terminal epitope [35], was used for immunodetection. The linear range of the chemiluminescence signal compared with the amount of protein on the gel has been determined for each cleavage product analysed.

First, we analysed the high-molecular mass products of Vi-induced photocleavage performed at 0 °C, using 7.5 % polyacrylamide gels and immunoblotting. As shown in Figure 1(A), human MRP1 migrates as a 160 kDa protein, and UV illumination alone causes no detectable peptide backbone cleavage (Figure 1A, lane 1). When Vi (800 μM) was present in the reaction mixture (Figure 1A, lanes 2–6) a specific cleavage product was formed. If no nucleotide was included in the reaction, a 95 kDa cleavage product, well recognized by the C-terminal antibody, was apparent (Figure 1A, lane 2). However, when MgATP (50 μM, lane 4) was included in the reaction mixture, the amount of the 95 kDa product was strongly decreased. Inhibition of the formation of the 95 kDa cleavage product was also observed when a non-hydrolysable ATP analogue, MgAMP-PCP (200 μM) (Figure 1A, lane 6), was included in the reaction. The presence of low concentration (1 μM) of either MgATP (Figure 1A, lane 3) or MgAMP-PCP (Figure 1A, lane 5) had no detectable effect on the Vi-induced cleavage reaction. In the following, we call Site I the Vi-cleavage site of MRP1 yielding this 95 kDa C-terminal fragment.

In the following experiments, we carried out the Vi-induced cleavage reactions at 37 °C (Figure 1B). Cleavage at Site I, resulting in the 95 kDa product, was also detected under these conditions. Again, in the presence of 50 μM MgATP or 200 μM MgAMP-PCP (Figure 1B, lanes 4 and 6 respectively), the concentration of the 95 kDa product was significantly lower than in the absence of nucleotide (Figure 1B, lane 2), or when only 1 μM of either nucleotide was present during the photo-cleavage reaction (Figure 1B, lanes 3 and 5).

As shown in Figure 1(B), in these experiments, we observed a new cleavage product of MRP1, with an apparent molecular mass of 85 kDa, recognized with the C-terminal antibody. MRP1 cleavage at Site II required the presence of MgATP (50 μM) (Figure 1B, lane 4). The 85 kDa cleavage product was absent when 200 μM (Figure 1B, lane 6) or 1 μM (Figure 1B, lane 5) MgAMP-PCP, or when only 1 μM MgATP (Figure 1B, lane 3) was included in the reaction mix. If magnesium ions were chelated by EDTA (100 μM) (Figure 1B, lane 7), the effect of the nucleotide at both Site I and Site II cleavage was mostly eliminated.

In the next set of experiments, we investigated the MRP1-cleavage products of lower molecular masses. The reaction products were analysed by immunoblotting from 15 % polyacrylamide gels, and again, the C-terminally reacting monoclonal antibody M6 was used. As shown in Figure 1(C), a cleavage product of MRP1 with an apparent molecular mass of 25 kDa was detected in the presence of 1 μM MgATP (Figure 1C, lane 3) or 1 μM MgAMP-PCP (Figure 1C, lane 5) at 0 °C. In the following, we call this cleavage site, generating a 25 kDa C-terminal fragment, Site III. When we examined further the effects of nucleotides on Vi cleavage at Site III, we found unexpectedly that, in the presence of 50 μM MgATP (Figure 1C, lane 4) or 50 μM MgAMP-PCP (Figure 1C, lane 6), very little, if any, cleavage product was generated. The same 25 kDa product could be detected in the absence of added nucleotide (Figure 1C, lane 2); however, the amount of the 25 kDa product was much less in the absence of

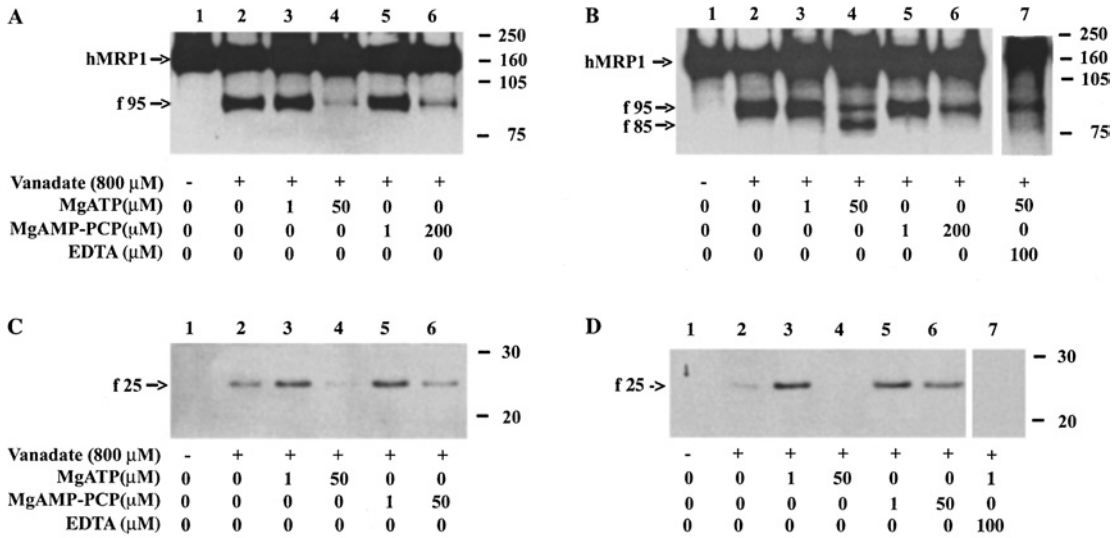

Figure 1 Nucleotide-dependent Vi-induced photo-oxidative cleavage in the N-proximal and in the C-proximal half of MRP1

Vi-induced photo-oxidative cleavage reactions were performed as described in the Materials and methods section. Arrow indicates the mature 160 kDa MRP1 protein. Arrows (f95, f85 and f25) indicate the position of cleavage products resulting in fragments with apparent molecular masses of 95 kDa, 85 kDa and 25 kDa respectively. The positions of the size markers are indicated at the right. (**A**) Cleavage reactions in the N-proximal half of MRP1 performed at 0 °C. Lane 1, photocleavage reaction without Vi and nucleotides; lanes 2–6, products of cleavage reactions in the presence of 0.8 mM Vi, and nucleotides as indicated below the immunoblots. (**B**) Cleavage reactions in the N-proximal half of MRP1 performed at 37 °C. The same reaction conditions were used as in the experiments shown in (**A**); lane 7, photocleavage reaction in the presence of 50 μM MgATP and 100 μM EDTA. (**C**) Cleavage reactions in the C-proximal half of MRP1 performed at 0 °C. Lane 1, photocleavage reaction without Vi; lanes 2–6, product of cleavage reaction in the presence of 0.8 mM Vi, and nucleotides as indicated below the immunoblots. (**D**) Cleavage reactions in the C-proximal half of MRP1 performed at 37 °C. The same reaction conditions were used as in the experiments shown in (**C**); lane 7, photocleavage reaction in the presence of 1 μM MgATP and 100 μM EDTA.

nucleotide than in the presence of 1 μM nucleotide (Figure 1C, compare lanes 2 and 3). Similar results were obtained for Site III cleavage when the reactions were performed at 37 °C (Figure 1D). Removal of magnesium ions with 100 μM EDTA also suppressed the photo-oxidative reaction at Site III in the presence of 1 μM ATP (Figure 1D, lane 7) or 1 μM MgAMP-PCP (results not shown). Similar effects were obtained when the experiments were performed at 0 °C (results not shown). We concluded that cleavage at Site III is triggered by low concentrations of nucleotide, and the weak signal in the absence of added nucleotide is probably due to traces of nucleotides present in the Sf9 cell-membrane preparation.

ΔMRP1, an inactive mutant of MRP1, lacking the N-terminal TMD0 and the L0 cytoplasmic loop, was also expressed in Sf9 cells, and membranes containing this protein were subjected to Vi-induced photo-oxidative cleavage (detailed results not shown). Analysis of the cleavage products obtained at 0 °C revealed that ΔMRP1 can be cleaved at Site I and peptide backbone cleavage at this site, similarly to that seen for MRP1, is inhibited by 50 μM MgATP or by 200 μM MgAMP-PCP. Low concentrations of either nucleotide had no detectable effect on cleavage at Site I. When cleavage of ΔMRP1 was performed at 37 °C, identical cleavage reactions were observed as at 0 °C, and the formation of the 85 kDa fragment in ΔMRP1 was not observed. Thus, at Site II, Vi-cleavage could not be induced in ΔMRP1. ΔMRP1 was cleaved at Site III, and again, low concentration (1 μM) of nucleotide (MgATP or MgAMP-PCP) triggered a cleavage reaction at Site III, while at high concentrations of MgATP or MgAMP-PCP (50 μM and 50 μM respectively), cleavage of ΔMRP1 was absent, both at 37 °C and at 0 °C. When ΔMRP1 was subjected to Vi-induced cleavage (either at 37 °C or at 0 °C) under the 'Mg-free' experimental conditions, similar to that seen for MRP1, the effect of nucleotides on cleavage at Site I and at Site III were undetectable (results not shown).

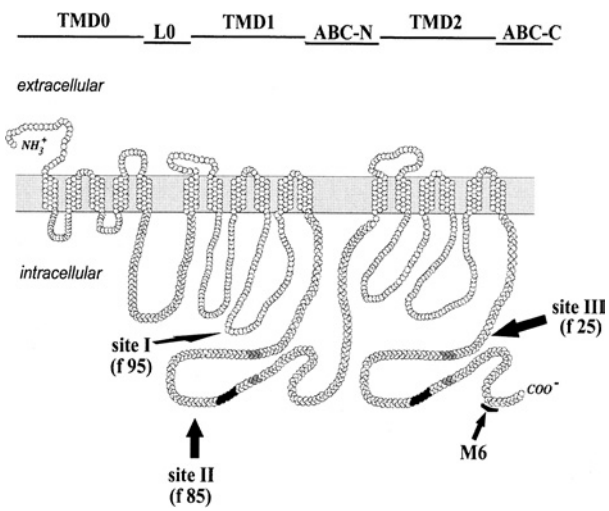

Figure 2 Membrane topology of MRP1 and localization of the cleavage sites

The membrane topology model of human MRP1 is based on that shown in [36]. The upper line indicates the arrangement of domains of MRP1 (L0 indicates the cytoplasmic loop connecting TMD0 and TMD1; ABC-N and ABC-C indicate the cytoplasmic ABC domains at the N- and the C-half of protein respectively). Arrows indicate cleavage at Site I, Site II and Site III at which Vi-induced cleavage reactions generate fragments of 95 kDa (f95), 85 kDa (f85) and 25 kDa (f25) respectively. Half-shaded regions of the polypeptide chain denotes the conserved Walker A and Walker B motifs, shaded regions show the ABC-signature motifs. The arrow with M6 points to the epitope of monoclonal antibody, M6.

On the basis of the estimated size of the cleavage products we mapped the approximate position of the cleavage sites within the linear sequence of MRP1. Figure 2 shows the membrane topology model and the domain arrangement of MRP1 [36], the

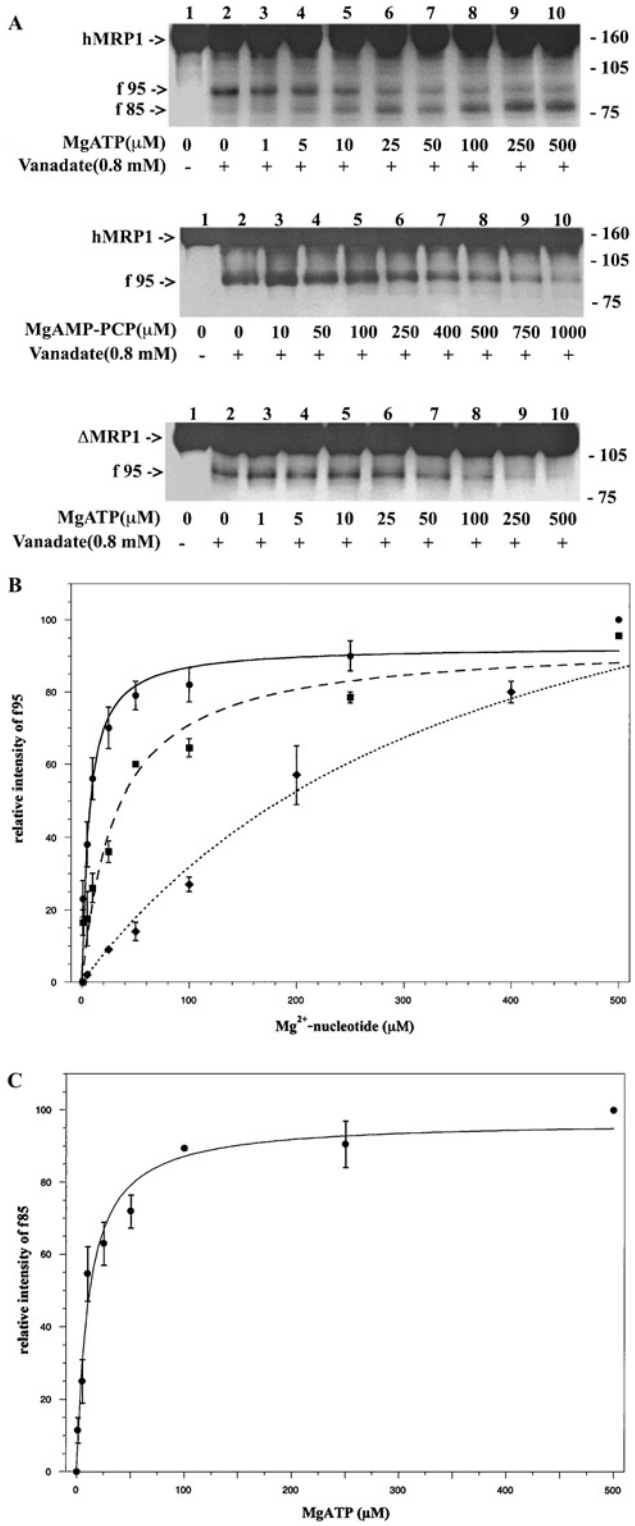

Figure 3 Nucleotide-dependent Vi-induced photo-oxidative cleavage reactions at the N-proximal half of MRP1 and that of ΔMRP1 at various nucleotide concentrations

Cleavage reactions were performed at 37 °C; the arrows (f95 and f85) indicate the cleavage products with molecular masses of 95 and 85 kDa respectively. (**A**) Immunoblots of cleavage reactions of MRP1 (upper panel) or that of ΔMRP1 (lower panel) performed in the presence of MgATP in concentrations as indicated below the immunoblots, and the immunoblots of cleavage reactions of MRP1 performed in the presence of MgAMP-PCP in concentrations as indicated below the immunoblots (middle panel). The absence or presence of Vi is indicated under the immunoblots. The positions of the molecular-mass markers are indicated at the right. (**B**) Densitometric evaluation of fragment f95 generated by cleavage reactions shown in (**A**). Data represent the means of at least three independent sets of experiments. The plot shows the extent of cleavage resulting fragment f95; densities measured in the cleavage reactions in the absence of nucleotide was arbitrarily set at 100. ●, MRP1 with MgATP; ■, ΔMRP1 with MgATP; ◆, MRP1 with MgAMP-PCP. (**C**) Densitometric evaluation of fragment f85 generated by cleavage reactions analysed in the upper panel of (**A**). Data represent the means of at least three independent sets of experiments. Data are expressed as relative density; densities measured in the cleavage reaction in the presence of 500 μM MgATP was arbitrarily set at 100.

position of the M6 epitope, and the putative sites of the Vi-induced photo-oxidative cleavage within the polypeptide chain. Site I, at which backbone cleavage generates the specific cleavage product of 95 kDa, can be assigned to the C-terminus of TMD1 (amino acids 317–611), or to the intracellular region (amino acids 612–649), which connects TMD1 to the N-proximal ABC domain. The 85 kDa product is generated by backbone cleavage at Site II, localized within the first ABC catalytic domain (amino acids 650–850). Site III, at which backbone cleavage generates the 25 kDa product, can be assigned to the C-proximal ABC domain (amino acids 1303–1531). In this case, a more refined localization is possible, since the disturbing effect of core glycosylation can be disclosed. Accordingly, the cleavage site must be at the N-terminal region (around position 1300) of the C-proximal ABC domain.

In order to analyse further the effects of nucleotides on the peptide backbone cleavage at Site I, at Site II and at Site III respectively, the Vi-cleavage reactions were performed in the presence of various concentrations of nucleotides at 37 °C. [We set the conditions of the cleavage reactions so that only a small portion (< 5 %) of the studied protein (MRP1 or ΔMRP1) was cleaved. Whether or not the rate of cleavage at Site II and at Site III are independent of the polypeptide chain cleavage at Site I, the generation of lower molecular mass fragments (i.e. the 85 kDa and the 25 kDa fragments) causes a smaller than 10 % error on the estimation of the yield of the 95 kDa fragment, and a smaller than 5 % error on the yield of the 85 kDa fragment. In the quantitative analysis, we neglected this potential error.] MRP1 was subjected to cleavage in the presence of MgATP (0–500 μM) (Figure 3A, upper panel) or in the presence of MgAMP-PCP (0–1000 μM) (Figure 3A, middle panel), or ΔMRP1 was cleaved in the presence of MgATP (0–500 μM) (Figure 3A, lower panel). When a quantitative evaluation of the concentration of the 95 kDa product was performed by densitometry, a nucleotide-concentration-dependent inhibition of cleavage of MRP1 at Site I was observed, with an apparent half-maximal effect at 6.6 ± 3.0 μM MgATP at 37 °C (Figure 3B). In contrast, MgATP triggered cleavage of MRP1 at 37 °C at Site II, and the half-maximal effect of the nucleotide was observed at 7.4 ± 3.6 μM MgATP concentration (Figure 3C). A concentration-dependent inhibition of cleavage of MRP1 at Site I was observed in the presence of MgAMP-PCP at 37 °C, with a half maximal inhibition at 128 ± 34 μM MgAMP-PCP (Figure 3B). The MgATP concentration-dependence of cleavage of ΔMRP1 at 37 °C was also analysed (Figure 3B). The MgATP concentration, causing a 50 % decrease in the cleavage of ΔMRP1 at Site I was 32.3 ± 4.1 μM.

Figure 4 shows the nucleotide-concentration-dependence of cleavage at Site III at 37 °C. The results indicate that a low concentration of MgATP (0.1 μM) triggers cleavage at Site III in MRP1, and the yield of the cleavage product increases up to 1 μM MgATP (Figure 4A, upper panel). Thereafter, the yield of cleavage decreases gradually as the concentration of MgATP is increased, and, in the presence of 50 μM MgATP, practically no cleavage was detected. In the presence of MgAMP-PCP, an essentially similar concentration-dependence of cleavage of MRP1 at Site III

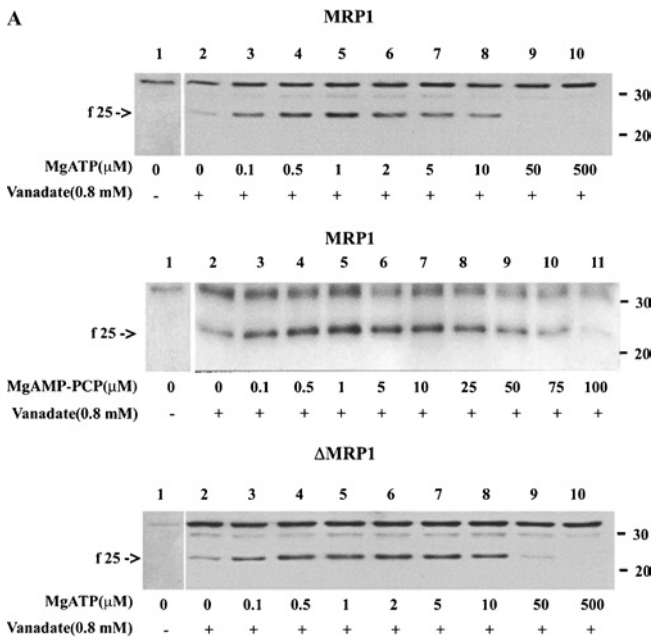

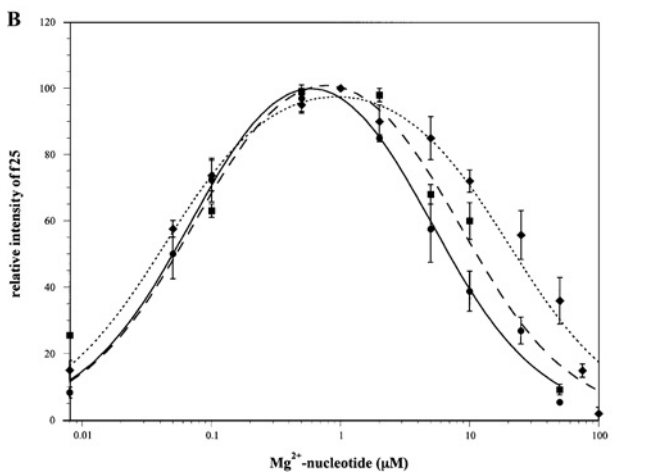

Figure 4 Nucleotide-dependent Vi-induced photo-oxidative cleavage reactions at the C-proximal half of MRP1 and that of ΔMRP1 at various nucleotide concentrations

Cleavage reactions were performed at 37 °C; the arrow indicates the cleavage product with molecular mass of 25 kDa (f25). (**A**) Immunoblots of cleavage reactions of MRP1 (upper panel) or that of ΔMRP1 (lower panel) performed in the presence of MgATP in concentrations as indicated below the immunoblots, and the immunoblots of cleavage reactions of MRP1 performed in the presence of MgAMP-PCP in concentrations as indicated below the immunoblots (middle panel). The absence or presence of Vi is indicated under the immunoblots. The positions of the molecular-mass markers are indicated on the right. (**B**) Densitometric evaluation of fragment f25 generated by cleavage reactions shown in (**A**). Data represent the mean of at least three independent sets of experiments. The plot shows the extent of cleavage resulting in fragment f25; densities measured in the cleavage reactions in the presence of 1 μM MgATP was arbitrarily set to 100. ●, MRP1 with MgATP; ■, ΔMRP1 with MgATP; ◆, MRP1 with MgAMP-PCP.

was observed (Figure 4A, middle panel), as in the case of MgATP. The relationship between cleavage of ΔMRP1 at Site III and MgATP concentration (Figure 4A, lower panel) was found to be similar to that observed when MRP1 was subjected to cleavage in the presence of MgATP.

A quantitative evaluation of the 25 kDa product by densitometry in the Vi-induced cleavage reactions showed a biphasic effect of the nucleotide concentration. This analysis also revealed certain

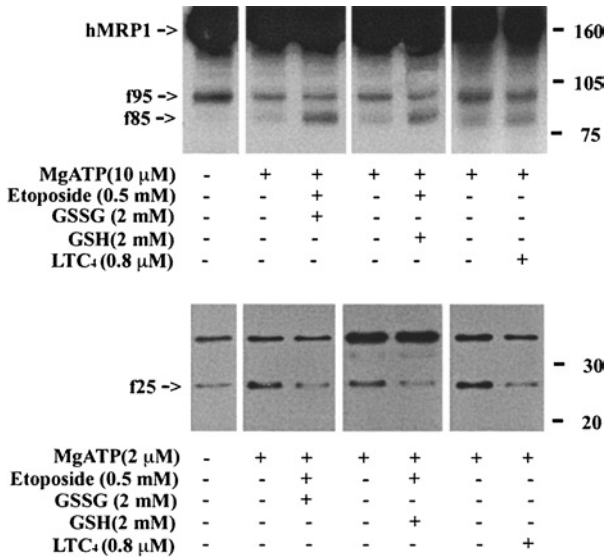

Figure 5 Effect of various transported substrates on the Vi-induced cleavage reactions at the N- and C-proximal halves of MRP1

Cleavage reactions were performed in the presence of various transported substrates and different concentrations of MgATP, as indicated below the immunoblots. Products generated by cleavage reactions at the N-proximal half of MRP1 are shown in the upper panels; those generated by cleavage reactions at the C-proximal half of MRP1 are shown in the lower panels. Arrows indicate the position of cleavage products resulting fragments with apparent molecular masses of 95 kDa, 85 kDa and 25 kDa (f95, f85 and f25 respectively). The positions of the molecular-mass markers are indicated on the right.

differences in the nucleotide-sensitivity of cleavage at Site III in MRP1 as compared with ΔMRP1, and when MRP1 was cleaved in the presence of MgATP or MgAMP-PCP respectively (Figure 4B). Deconvolution of the bell-shape curves revealed the following half-maximal concentration values: 0.07 ± 0.01 μM and 4.5 ± 0.6 μM MgATP for the rising and declining parts of the curve respectively, in the case of cleavage of MRP1 in the presence of MgATP; 0.07 ± 0.01 μM MgATP and 8.0 ± 2.8 μM MgATP for the rising and declining parts of the curve respectively, in the case of ΔMRP1, in the presence of MgATP; 0.04 ± 0.01 μM MgAMP-PCP and 19.7 ± 3.7 μM MgAMP-PCP for the rising and declining parts of the curve respectively, in the case of MRP1, in the presence of MgAMP-PCP. Similar results were obtained for the Site III cleavage of MRP1 at 0 °C in the presence of either MgATP or MgAMP-PCP, or when ΔMRP1 was subjected to cleavage in the presence of MgATP (results not shown).

Next, we investigated the effects of transported substrates on the Vi-induced cleavage reactions, observed at various sites, as described above. Several different substrates or substrate combinations, LTC_4 (leukotriene C_4; 800 nM), etoposide (500 μM), verapamil (150 μM), GSSG (2 mM), GSH (2 mM), etoposide (500 μM) + GSSG (2 mM), and etoposide (500 μM) + GSH (2 mM) were used in these experiments. The presence of etoposide (500 μM), verapamil (150 μM), GSSG (2 mM) or GSH (2 mM) had no effect on the cleavage reactions of MRP1 (results not shown).

Figure 5 shows the effects of LTC_4 (800 nM), etoposide (500 μM) + GSSG (2 mM), and etoposide (500 μM) + GSH (2 mM) on the Vi-induced cleavage reactions at the different cleavage sites. No effect of the transported substrates on the cleavage reactions at Site I, resulting in the 95 kDa fragment, could be observed (Figure 5, upper panel). However, a significant increase in the yield of cleavage at Site II (performed in the presence of

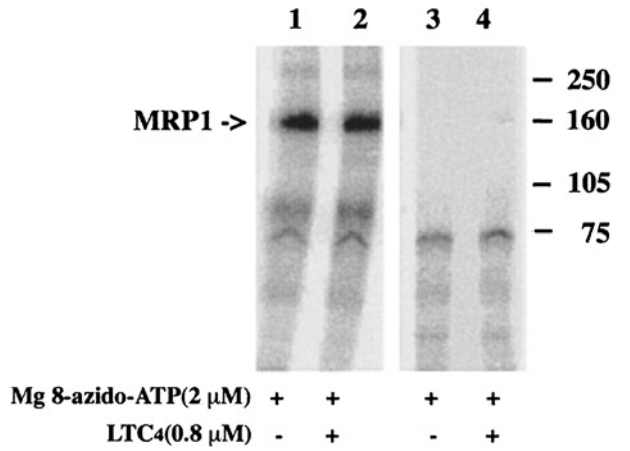

Figure 6 Effect of LTC_4 on nucleotide binding by MRP1

Autoradiogram of photolabelling of MRP1- (lanes 1 and 2) and β-galactosidase- (lanes 3 and 4) expressing Sf9 membranes. The photo-cross-linking reactions were performed in the presence of 8-azido-ATP (2 μM) and in the absence (lanes 1 and 3) or presence (lanes 2 and 4) of LTC_4 (0.8 μM). The positions of the molecular-mass markers are indicated on the right.

10 μM MgATP), resulting in the 85 kDa fragment was detected in the presence of each of the above substrates (Figure 5, upper panel). No cleavage at Site II was observed at 0 °C in the presence of any of the substrates or when MgATP was replaced with MgAMP-PCP, or when ΔMRP1 was subjected to the cleavage reaction in the presence of MgATP (results not shown).

As shown in Figure 5 (lower panel), the extent of cleavage at Site III, generating the 25 kDa fragment, was decreased in the presence of the MRP1 substrates. These experiments were performed in the presence of 2 μM MgATP.

In order to analyse further the effect of transported substrate on nucleotide binding, we used radiolabelled 8-azido-ATP and photo-cross-linking methodology. First, we determined the linear range of 8-azido-ATP concentration compared with the extent of photo-cross-linking, as determined by autoradiography on a phosphoimager. We have found that the incorporated radioactivity showed a linear function of concentration up to 5 μM 8-azido-ATP (results not shown). The effect of transported substrate on nucleotide binding was studied in the presence of 2 μM 8-azido-ATP and 0.8 μM LTC_4 (Figure 6). As a control, Sf9 membranes of cells expressing β-galactosidase were also subjected to 8-azido-ATP photolabelling in the absence and in the presence of 0.8 μM LTC_4 (Figure 6, lanes 3 and 4). The results shown in Figure 6 demonstrate that 0.8 μM LTC_4 had no effect on the extent of 8-azido-ATP photolabelling of MRP1 (Figure 6, lanes 1 and 2), as the same amount of incorporated radioactivity was found both in both the presence and the absence of the transported substrate, LTC_4.

Figure 7(A) shows the MgATP-concentration-dependence of cleavage at Site I and at Site II at 37 °C, in the absence (Figure 7A, upper panel) and in the presence of etoposide (500 μM) +GSSG (2 mM) (Figure 7A, lower panel). We found that the transported substrates stimulated the cleavage reaction at Site II, whereas they had no effect on the reaction at Site I. The results of the quantitative evaluation of the concentration of the 85 kDa product by densitometry, plotted against MgATP concentration are shown in Figure 7(B). These plots indicate a 3- to 4-fold increase of the cleavage yield, with no significant change in the concentrations resulting in the half-maximal effect of the nucleotide (4.0 ± 0.8 μM compared with 7.4 ± 3.6 μM MgATP), in the presence of the transported substrates.

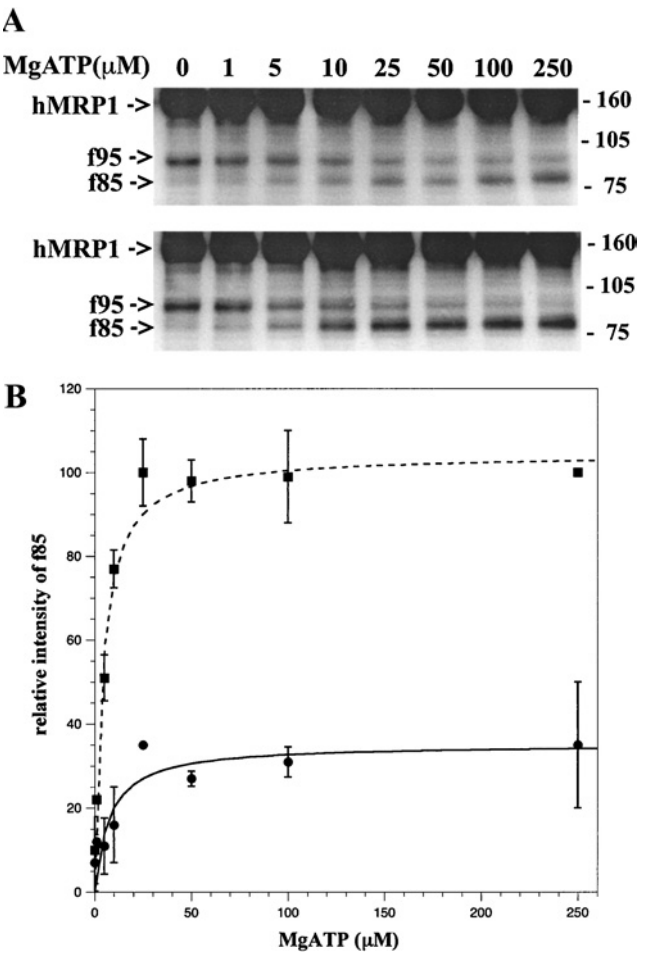

Figure 7 Effect of etoposide and GSSG on the Vi-induced cleavage reaction at the N-proximal half of MRP1

(**A**) Vi-induced cleavage reactions were performed in the absence (upper panel) and in the presence (lower panel) of etoposide (0.5 mM) and GSSG (2 mM) at various MgATP concentrations as indicated above the immunoblots. Arrows indicate the position of cleavage products resulting in fragments with apparent molecular masses of 95 kDa and 85 kDa (f95 and f85 respectively). The positions of the molecular-mass markers are indicated on the right. (**B**) Densitometric evaluation of fragment f85 generated by cleavage in the presence (■) or in the absence (●) of etoposide (0.5 mM) and GSSG (2 mM) at various MgATP concentrations. Data are expressed as relative densities; densities measured in the cleavage reaction in the presence of 250 μM MgATP and etoposide (0.5 mM) + GSSG (2 mM) were arbitrarily set at 100. Data represent the mean of at least three independent sets of experiments.

Figure 8(A) shows the MgATP-concentration-dependence of cleavage of MRP1 at Site III at 37 °C, in the absence and in the presence of etoposide (500 μM) +GSSG (2 mM) in the concentration range 0–1 μM (Figure 8A, upper panel) and 2–50 μM (Figure 8A, lower panel) MgATP. At each MgATP concentration, a significant decrease of the cleavage yield was observed when the reaction was performed in the presence of the transported substrate. The results of the quantitative evaluation of the 25 kDa product, obtained in the presence or in the absence of etoposide (500 μM) +GSSG (2 mM) are shown in Figure 8(B). The plots show a biphasic, bell-shaped function of cleavage against MgATP concentration, both in the absence and in the presence of etoposide + GSSG. However, the declining part of the curve is shifted towards lower MgATP concentrations (4.5 ± 0.6 μM compared with 1.2 ± 0.4 μM MgATP) in the presence of the transported substrates.

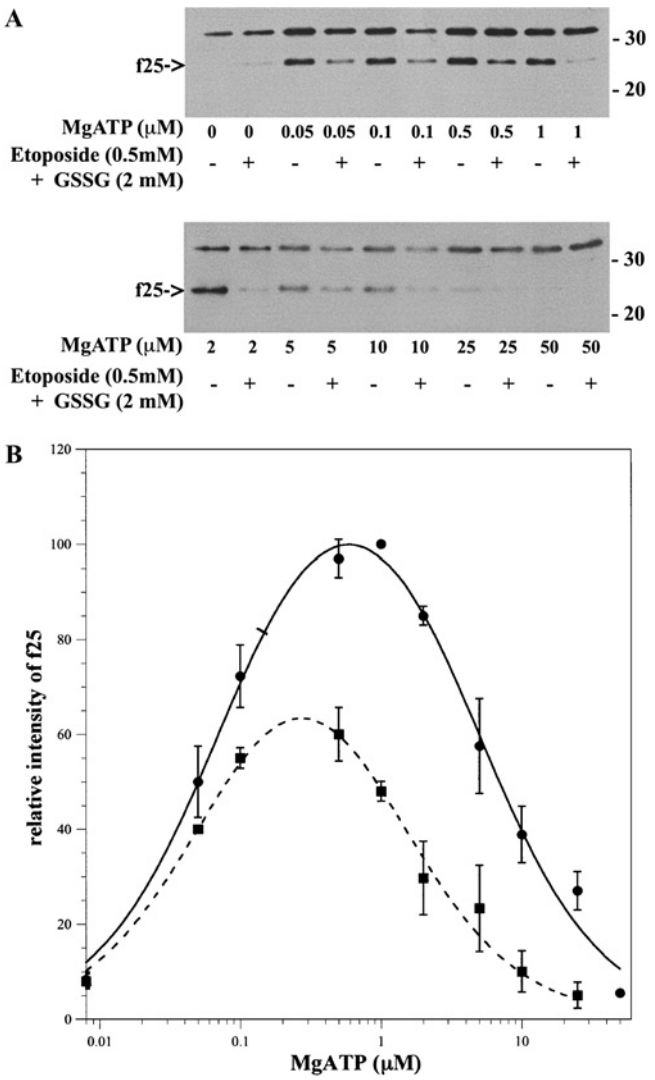

Figure 8 Effect of etoposide and GSSG on the Vi-induced cleavage reaction at the C-proximal half of MRP1

(**A**) Vi-induced cleavage reactions were performed at 37 °C in the absence and in the presence of etoposide (0.5 mM) and GSSG (2 mM) at various MgATP concentration as indicated below the immunoblots. Arrow indicates the position of cleavage product resulting in fragment with apparent molecular mass of 25 kDa (f25). The positions of the molecular-mass markers are indicated on the right. (**B**) Densitometric evaluation of fragment f25 generated by cleavage in the presence (■) or in the absence (●) of etoposide (0.5 mM) and GSSG (2 mM) at various MgATP concentrations. Data are expressed as relative densities; densities measured in the cleavage reaction in the presence of 1 μM MgATP (in the absence of etoposide + GSSG) were arbitrarily set at 100. Data represent the mean of at least three independent sets of experiments.

No effect of etoposide + GSSG was observed on cleavage at Site III in ΔMRP1, or in MRP1 in the presence of the non-hydrolysable nucleotide, MgAMP-PCP (0.05–100 μM), at 37 °C. Similarly, no effect was found when cleavage of MRP1 was performed at 0 °C in the presence of MgATP (0.05–100 μM) (results not shown).

DISCUSSION

In the present study, we have detected three sites within the MRP1 protein, at which Vi induced a photo-activated cleavage of the peptide backbone (see Figure 2). We found that cleavage at these sites detected major conformational changes during the catalytic cycle due to the interactions of the MRP1 with MgATP and with the transported substrates.

When analysing the Vi-dependent cleavage of MRP1, we found that cleavage at Site I was inhibited by nucleotides (Figures 1 and 3). Our results indicate that this inhibition is caused by specific nucleotide binding (and/or by formation of a pre-hydrolytic complex) in the ABC domain. This is supported by the following findings: (i) both MgATP and its non-hydrolysable analogue, MgAMP-PCP, influenced cleavage at this site (see Figures 1A and 1B); (ii) the nucleotide-sensitivity of cleavage at Site I in ΔMRP1 was similar to that in the wild-type MRP1 (this inactive mutant of MRP1 binds MgATP similarly to the wild-type MRP1, but transition-state formation is absent [34]); (iii) the effect of nucleotides could also be detected at 0 °C, which indicates that no hydrolytic event was taking place (Figure 1A). However, the nucleotide-dependence of cleavage at Site I in MRP1 in the presence of MgATP or MgAMP-PCP are different (Figure 3A, upper and middle panels); the same is true if the nucleotide-dependence of cleavage at Site I of MRP1 is compared with that of ΔMRP1 (Figure 3A, lower panel).

The most plausible explanation for the nucleotide-induced inhibition of Vi-cleavage at Site I is that major conformational changes occur at this site upon nucleotide binding and/or upon the formation of a pre-hydrolytic intermediate. It has been already documented that the TMDs of MDR1 undergo major rearrangement upon nucleotide binding [38,39], and the same phenomenon may occur in MRP1 as well. Interestingly, transported-substrate binding to MRP1 did not influence the Vi-dependent cleavage at Site I (Figure 5).

Another photo-oxidative cleavage reaction site in MRP1, termed Site II, found within the N-proximal ABC unit, behaved entirely differently. We suggest that Vi resides here in the active site, as a part of the MRP1 · MgADP · Vi complex ('trapped nucleotide'). The following experimental data support this conclusion: (i) cleavage at Site II occurs only in the presence of MgATP (see Figure 1B, lane 4), but not in the presence of the non-hydrolysable analogue, MgAMP-PCP (see Figure 1B, lane 6). The former nucleotide can form an MRP1 · MgADP · Vi complex after hydrolysis [17,34], while MgAMP-PCP cannot participate in such a complex; (ii) the inactive mutant, ΔMRP1, is not able to form the MRP1 · MgADP · Vi complex [34], and we detected no cleavage at Site II in this MRP1-mutant; and (iii) photocleavage at Site II was not observed at 0 °C, but could be detected at 37 °C, under conditions that favour hydrolysis (compare Figure 1A, lane 4, with Figure 1B, lane 4).

A third Vi-cleavage site, Site III, was found in the C-proximal ABC-domain. As demonstrated in Figures 1(C) and 1(D), the Vi-induced photo-cleavage at this site was influenced by specific nucleotide binding (and by the formation of a pre-hydrolytic complex; see below). Experimental data supporting this conclusion are the same as described for cleavage at Site I. Following this line of reasoning, the formation of the post-hydrolytic MRP1 · MgADP · Vi complex ('trapped nucleotide') could not be detected directly by photo-cleavage reaction at this nucleotide-interacting site.

To summarize, we found that cleavage at Site II is ADP · Vi-dependent, (i.e. it requires the formation of the MRP1 · MgADP · Vi post-hydrolytic complex). This means that Vi-cleaving of the peptide backbone is induced by this trapped complex. On the other hand, cleavage at Site I and at Site III does not require the formation of such a complex, and the yields of these reactions are modulated by pre-hydrolytic events (nucleotide binding and/or pre-hydrolytic complex formation). Consequently, the

effects of nucleotides on cleavage at Sites I and III come from the conformational changes induced by these pre-hydrolytic events.

According to the current structural model, based on X-ray crystallographic data of bacterial ABC ATPases [10–14], the two ABC units form two composite active centres. This means that elements of both ABC units participate in the formation of the two catalytic centres. Therefore it is difficult to delineate the different functional characteristics of the composite sites (made from elements of both ABC domains) to the domains in the linear polypeptide chain sequence, where Vi-induced cleavage is observed.

We have found that the nucleotide sensitivity of the various MRP1–nucleotide interactions detected by Vi-cleavage at the N-proximal and at the C-proximal halves were significantly different (for the sake of simplicity in the following, we refer to the active sites as 'N-proximal' and 'C-proximal', which indicates, however, only the location of the Vi-cleavage sites). Nucleotide binding and/or pre-hydrolytic intermediate (Site I) and MRP1 · MgADP · Vi 'trapped' inhibitory complex formation (Site II), detected by cleavage in the N-proximal half, were saturable at increasing nucleotide concentrations (see Figure 3). The MgATP concentrations that yielded a half-maximal effect in this interaction were estimated to be approx. 6.6 and 7.4 μM respectively.

In contrast, the nucleotide-binding site detected by Vi-induced cleavage at Site III had a much higher nucleotide affinity and could not be saturated by MgATP (Figure 4). Deconvolution of the biphasic concentration-dependence of the nucleotide-effect on the cleavage reaction at Site III revealed that the half maximal effect is caused by about 0.1 μM MgATP on the rising part of the curve (which detects nucleotide binding; see Figure 4B). The biphasic nature of the nucleotide concentration of the cleavage reaction at Site III could be interpreted to mean that a MRP1–nucleotide interaction at a different site of the protein has a major impact on the nucleotide-binding properties detected at Site III. The half-maximal MgATP concentration of the declining part of the curve (an apparent 'inhibition') at this site was found to be approx. 4.5 μM. The calculated value is similar to the half-maximally effective concentration of MgATP at Site I (6.6 μM), which can be associated to the LAS. These data support the suggestion that binding of a nucleotide to the LAS has an allosteric effect on the HAS.

It is worthwhile to note that the nucleotide-concentration-dependence of cleavage at Site III of ΔMRP1 shows a similar biphasic function to that of MRP1 (Figure 4B). Similarly to that for MRP1, the half-maximal effect is caused by approx. 0.07 μM MgATP at the rising part of the curve, while the 'inhibition' of cleavage in MRP1 and ΔMRP1 are different (4.5 μM and 8 μM). Similar phenomena have been observed when cleavage of MRP1 was performed in the presence of MgAMP-PCP (Figure 4). The concentrations of the half-maximal effect of binding (as determined for the rising part of the curves) are similar, while those of 'inhibition' of cleavage of MRP1 in the presence of MgATP or MgAMP-PCP are different (4.5 μM and 20 μM respectively).

In summary, higher values measured for the effects of nucleotides at Site I (Figure 3B) are accompanied by higher values of the declining part of the nucleotide-concentration curve at Site III (Figure 4B). This observation reinforces our interpretation above that binding of nucleotide to one of the sites has an effect on the state of the nucleotide at the other site. At low MgATP concentration, the nucleotide binds to a site which can be detected by cleavage at Site III, as the rising part of the concentration curve. At higher concentrations, nucleotide binds to the other binding site too (which is detected by cleavage at Site I), and this binding triggers a conformational change reducing the binding of a nucleotide to the HAS (detected as the declining part of the curve).

These results are in harmony with the current hypothesis that nucleotide–protein interaction detected at one of the sites accelerates the catalytic reaction at the other site; a conclusion that has been obtained by utilizing azido-nucleotide-trapping experimental strategies [25,27]. These authors found that saturation of the ATP-binding site in the N-ABC domain enhanced the formation of the MRP1 · MgADP · Vi complex (i.e. the post-hydrolytic complex) in the C-ABC domain. Our similar results mean that the experimental strategy based on the Vi-induced polypeptide-backbone cleavage is suitable for investigating the mechanism of the hydrolytic cycle of MRP1 [as we mentioned above, it is difficult to identify the LAS and HAS with either the N-ABC or with the C-ABC, as the nucleotide-interacting sites/catalytic centres of the ABC ATPases are composed of polypeptide segments from both ABC domains ('composite sites')]. Our data obtained by the Vi-cleavage technique have led to several new findings. They indicate that the target of the positive allosteric effect of the nucleotide is a step in the catalytic cycle preceding the cleavage of the phosphodiester bond between the β and the γ phosphate of ATP, i.e. the formation of a pre-hydrolytic complex. This is supported by the following experimental data: (i) MgATP and its non-hydrolysable analogue (MgAMP-PCP) show similar biphasic effects on the cleavage reaction at Site III (Figure 4); (ii) the inactive mutant of MRP1, ΔMRP1 (in which no enzyme · MgADP · Vi post-hydrolytic inhibitor complex can be formed) shows the same biphasic nucleotide-concentration-dependence of cleavage at Site III as MRP1 (Figure 4); and (iii) similar nucleotide-concentration-dependence of the cleavage was detected at 0 °C and at 37 °C. On the basis of the above observations, we could refine the target of this positive allosteric event in the catalytic cycle: we concluded that the enhancement of activity at the catalytic centre associated with the HAS is due to the accelerated conversion of the bound nucleotide state into a pre-hydrolytic intermediate state.

Compounds transported by ABC transporters accelerate the initial rate of ATP hydrolysis [31,37,40], and it was also shown that these compounds accelerate the rate of formation of the MRP1 · MgADP · Vi post-hydrolytic inhibitor complex, as detected by Mg-azido-ATP trapping [17,18,24,34]. We found that the interaction of MRP1 with its transported substrates had no effect on the Vi-induced cleavage at Site I (Figures 5 and 7). As discussed above, cleavage at Site I is influenced by specific nucleotide binding (and/or by formation of a pre-hydrolytic complex). Therefore our data suggest that the transported substrates have no effect on nucleotide binding and/or on the formation of a pre-hydrolytic complex. To establish further this conclusion, we performed direct nucleotide-binding experiments in the presence and absence of a transported substrate. As shown in Figure 6, LTC_4 had no effect on the extent of 8-azido-ATP photolabelling of MRP1. Thus the results obtained by an independent experimental approach fully support the above conclusion.

We have found that Vi-cleavage reactions at Site II and at Site III were sensitive to the substrate–transporter interaction (see Figures 5, 7 and 8). As discussed above, cleavage at Site II (similarly to Mg-azido-ATP trapping) detects the posthydrolytic complex formation. Accordingly, the transported substrates stimulate the formation of such a complex, as detected by cleavage at Site II.

Cleavage of MRP1 at Site III was also sensitive to the transported substrates; i.e. the declining part of the curve was significantly shifted toward lower MgATP concentrations in the presence of substrates (Figure 8B). This effect was observed only if the reaction was performed under hydrolytic conditions; i.e.

in the presence of MgATP at 37 °C, and not in the presence of MgAMP-PCP or at 0 °C. Cleavage of the inactive ΔMRP1 at Site III was insensitive to the presence of transported substrates.

As we interpreted the declining part of the curve as conversion of the bound nucleotide state into a pre-hydrolytic state (see above), the left-shift in this phase in the presence of transported substrates under hydrolytic conditions detects the conversion of the pre-hydrolytic complex into the post-hydrolytic enzyme · MgADP · Vi complex, and this reaction is the target of substrate-induced allosteric effect, which is detected as Site III cleavage.

Another novel finding revealed by Vi-mediated cleavage reactions was the formation of the MRP1–MgADP–Vi post-hydrolytic intermediate complex in both catalytic centres. Furthermore, we could show that interaction of the transporter with its transported substrates had a positive allosteric impact in both catalytic sites on the post-hydrolytic intermediate formation.

Consequently, the results described in the present paper indicate that the two different allosteric effects observed in the MRP1 ATPase cycle control two different steps of the catalysis. The nucleotide-binding-induced allosteric effect accelerates a pre-hydrolytic complex formation, which involves communication between the two catalytic centres, whereas interaction with the transported substrates stimulates a later reaction step of the hydrolytic cycle, the formation of the post-hydrolytic intermediate in both catalytic centres.

Based on the results discussed above, a model has been developed to describe the different conformational states and the transitions detected in MRP1 (see Scheme 1). Since, in the presence of Vi, MRP1 is trapped in an inhibitory complex state and the catalytic cycle is arrested, we could analyse the model at equilibrium (see the Materials and methods section). The model includes the binding of a nucleotide first to a HAS, followed by the second nucleotide binding to a LAS. This later binding triggers a conformational change resulting in pre-hydrolytic intermediate state formation at the HAS. In analogy with the experimental observation in MDR1 [21], we made the following assumption: in each MRP1 molecule, at the same time, only one of the two catalytic centres can be present in the post-hydrolytic (enzyme · MgADP · Vi intermediate) complex form. Consequently, the reaction scheme ends with two different states; i.e. either the N-proximal or the C-proximal catalytic site of MRP1 is present in a post-hydrolytic intermediate state.

The mathematical analysis of this equilibrium model was based on the equations presented in the Materials and methods section. We calculated the normalized concentrations of fragments f95, f85 and f25, which we could detect in Vi-induced cleavage reactions at Site I, Site II and Site III respectively. Then we used a global fitting procedure, when the best fit was sought by adjusting the parameters of the model (the intrinsic equilibrium constants) to accommodate simultaneously all the experimental cleavage data. Figure 9 shows the theoretical curves determined by the global fitting of our model to the experimental data. The obtained intrinsic equilibrium constants for the individual reactions, defined in Scheme 1, are summarized in Table 1.

The calculations based on this simplified equilibrium model resulted in a remarkably good fit to the experimental data. This indicates that the model may properly describe the crucial features of the MRP1 ATPase catalytic cycle. Based on the model, the two nucleotide-binding sites show different MgATP affinities; the HAS is characterized by an intrinsic dissociation constant of 0.12 μM, whereas this value is 50 μM for the LAS. There is an allosteric interaction between the two nucleotide-binding sites, namely the binding of a nucleotide to the LAS generates a conformational change at the occupied HAS, and accelerates its conversion into a pre-hydrolytic intermediate.

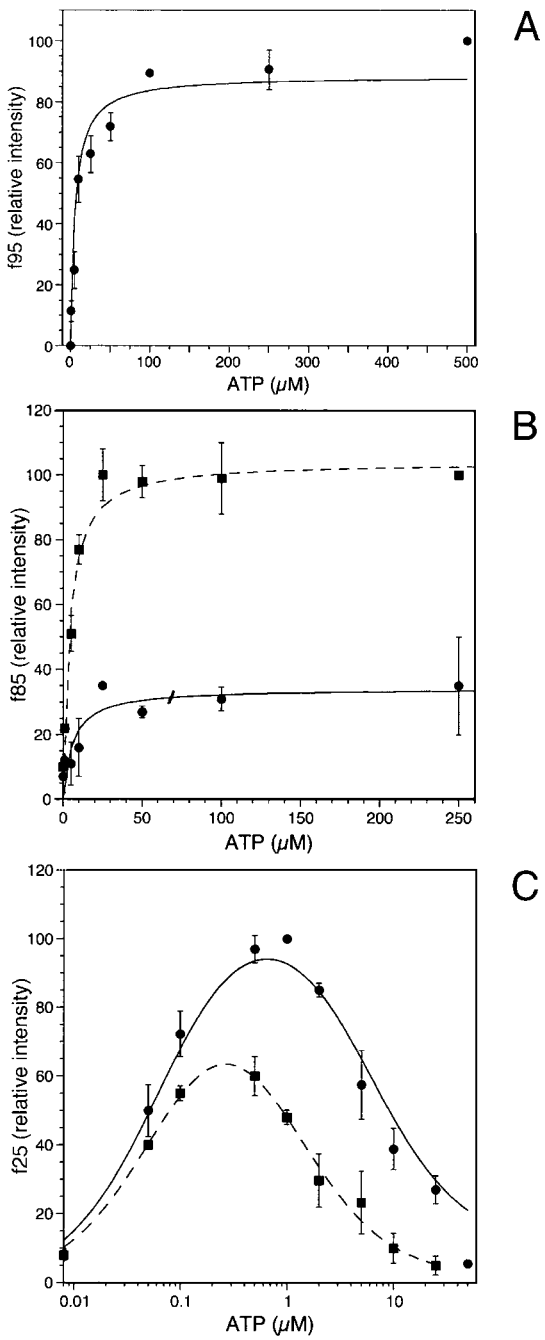

Figure 9 Global fit of the equilibrium model

Theoretical curves obtained by global fitting the model parameters to the experimental data. Based on our equilibrium model (see Scheme 1), we estimated the intrinsic association constants K_H and K_L and the isomerization constants K_{Pre}, $K_{Post}{}^H$ and $K_{Post}{}^L$ (for definitions, see the Materials and methods section) of the MRP1 ATPase cycle reactions involved in the model by minimizing the sum of φ^2 values of the individual fits of f95, f85 and f25 functions (eqns 3–5) to data presented in Figures 3, 4, 7 and 8, in the absence and presence of transported substrate. In the presence of transported substrate, only the isomerization constants characterizing the pre-hydrolytic to post-hydrolytic intermediate transitions ($K_{Post}{}^H$ and $K_{Post}{}^L$) were allowed to change [broken lines in (**B**) and (**C**)], the other parameters were the same as for the absence of transported substrate [solid lines in (**A**), (**B**) and (**C**)]. Theoretical curves for the ATP-concentration-dependence of fragments are shown for f95 in (**A**), for f85 in (**B**) and for f25 in (**C**).

Both catalytic centres of MRP1 are hydrolytically active, and the transported substrates have a positive allosteric effect on the conversion of a pre-hydrolytic into a post-hydrolytic intermediate

Table 1 Intrinsic equilibrium constants estimated by global fitting of the model

TS, transported substrate.

	Fragment				
Constant	f95	f85		f25	
TS	−/+	−	+	−	+
K_H (1/μM)	7.7	7.7	7.7	7.7	7.7
K_L (1/μM)	0.016	0.016	0.016	0.016	0.016
K_{Pre}	7	7	7	7	7
$K_{Post}{}^H$	0.2	0.2	0.2	0.2	7
$K_{Post}{}^L$	0.2	0.2	1	0.2	0.2

at both active centres. However, the different equilibrium constants obtained for the two sites indicate that post-hydrolytic intermediate formation in the two catalytic sites may be different.

This work was supported by research grants from OTKA (National Science Fund of Hungary) (T35126, T43448 and D35126) and by a NKFP (National Research and Development Fund of Hungary) 1/047 grant. B. S. is recipient of a Howard Hughes International Scholarship. The skilful technical help of Györgyi Demeter is gratefully acknowledged.

REFERENCES

1 Cremo, C. R., Grammer, J. C. and Yount, R. G. (1989) Direct chemical evidence that serine 180 in the glycine-rich loop of myosin binds to ATP. J. Biol. Chem. **264**, 6608–6611
2 Grammer, J. C., Loo, J. A., Edmonds, C. G., Cremo, C. R. and Yount, R. G. (1996) Chemistry and mechanism of vanadate-promoted photooxidative cleavage of myosin. Biochemistry **35**, 15582–15592
3 Smith, C. A. and Rayment, I. (1996) X-ray structure of the magnesium(II)–ADP–vanadate complex of the *Dictyostelium discoideum* myosin motor domain to 1.9 Å resolution. Biochemistry **35**, 5404–5417
4 Fisher, A. J., Smith, C. A., Thoden, J. B., Smith, R., Sutoh, K., Holden, H. M. and Rayment, I. (1995) X-ray structures of the myosin motor domain of *Dictyostelium discoideum* complexed with MgADP.BeFx and MgADP.AlF4-. Biochemistry **34**, 8960–8972
5 Daoud, R., Julien, M., Gros, P. and Georges, E. (2001) Major photoaffinity drug binding sites in multidrug resistance protein 1 (MRP1) are within transmembrane domains 10–11 and 16–17. J. Biol. Chem. **276**, 12324–12330
6 Haimeur, A., Deeley, R. G. and Cole, S. P. C. (2002) Charged amino acids in the sixth transmembrane helix of multidrug resistance protein 1 (MRP1/ABCC1) are critical determinants of transport activity. J. Biol. Chem. **277**, 41326–41333
7 Ito, K., Olsen, S. L., Qiu, W., Deeley, R. G. and Cole, S. P. C. (2001) Mutation of a single conserved tryptophan in multidrug resistance protein 1 (MRP1/ABCC1) results in loss of drug resistance and selective loss of organic anion transport. J. Biol. Chem. **276**, 15616–15624
8 Ren, X. Q., Furukawa, T., Aoki, S., Nakajima, T., Sumizawa, T., Haraguchi, M., Chen, Z. S., Kobayashi, M. and Akiyama, S. (2001) Glutathione-dependent binding of a photoaffinity analog of agosterol A to the C-terminal half of human multidrug resistance protein. J. Biol. Chem. **276**, 23197–23206
9 Karwatsky, J., Daoud, R., Cai, J., Gros, P. and Georges, E. (2003) Binding of a photoaffinity analogue of glutathione to MRP1 (ABCC1) within two cytoplasmic regions (L0 and L1) as well as transmembrane domains 10–11 and 16–17. Biochemistry **42**, 3286–3294
10 Hopfner, K. P., Karcher, A., Shin, D. S., Craig, L., Arthur, L. M., Carney, J. P. and Tainer, J. A. (2000) Structural biology of Rad50 ATPase: ATP-driven conformational control in DNA double-strand break repair and the ABC-ATPase superfamily. Cell **101**, 789–800
11 Locher, K. P., Lee, A. T. and Rees, D. C. (2002) The *E. coli* BtuCD structure: a framework for ABC transporter architecture and mechanism. Science **296**, 1091–1098
12 Smith, P. C., Karpowich, N., Millen, L., Moody, J. E., Rosen, J., Thomas, P. J. and Hunt, J. F. (2002) ATP binding to the motor domain from an ABC transporter drives formation of a nucleotide sandwich dimer. Mol. Cell **10**, 139–149
13 Chen, J., Lu, G., Lin, J., Davidson, A. L. and Quiocho, F. A. (2003) A tweezers-like motion of the ATP-binding cassette dimer in an ABC transport cycle. Mol. Cell **12**, 651–661
14 Chang, G. (2003) Structure of MsbA from *Vibrio cholera*: A multidrug resistance ABC transporter homolog in closed conformation. J. Mol. Biol. **330**, 419–430
15 Urbatsch, I. L., Sankaran, B., Weber, J. and Senior, A. E. (1995) P-glycoprotein is stably inhibited by vanadate-induced trapping of nucleotide at a single catalytic site. J. Biol. Chem. **270**, 19383–19390
16 Sankaran, B., Bhagat, S. and Senior, A. E. (1997) Inhibition of P-glycoprotein ATPase activity by beryllium fluoride. Biochemistry **36**, 6847–6853
17 Taguchi, Y., Yoshida, A., Takada, Y., Komano, T. and Ueda, K. (1997) Anti-cancer drugs and glutathione stimulate vanadate-induced trapping of nucleotide in multidrug resistance-associated protein (MRP). FEBS Lett. **401**, 11–14
18 Szabó, K., Welker, E., Bakos, É., Müller, M., Roninson, I., Váradi, A. and Sarkadi, B. (1998) Drug-stimulated nucleotide trapping in the human multidrug transporter MDR1: cooperation of the nucleotide binding domains. J. Biol. Chem. **273**, 10132–10138
19 Urbatsch, I. L., Sankaran, B., Bhagat, S. and Senior, A. E. (1995) Both P-glycoprotein nucleotide-binding sites are catalytically active. J. Biol. Chem. **270**, 26956–26961
20 Sauna, Z. E. and Ambudkar, S. V. (2000) Evidence for a requirement for ATP hydrolysis at two distinct steps during a single turnover of the catalytic cycle of human P-glycoprotein. Proc. Natl. Acad. Sci. U.S.A. **97**, 2515–2520
21 Hrycyna, C. A., Ramachandra, M., Ambudkar, S. V., Ko, Y. H., Pedersen, P. L., Pastan, I. and Gottesman, M. M. (1998) Mechanism of action of human P-glycoprotein ATPase activity: photochemical cleavage during a catalytic transition state using orthovanadate reveals cross-talk between the two ATP sites. J. Biol. Chem. **273**, 16631–16634
22 Hou, Y. X., Cui, L., Riordan, J. R. and Chang, X. B. (2000) Allosteric interactions between the two non-equivalent nucleotide binding domains of multidrug resistance protein MRP1. J. Biol. Chem. **275**, 20280–20287
23 Gao, M., Cui, H. R., Loe, D. W., Grant, C. E., Almquist, K. C., Cole, S. P. C. and Deeley, R. G. (2000) Comparison of the functional characteristics of the nucleotide binding domains of multidrug resistance protein 1. J. Biol. Chem. **275**, 13098–13108
24 Nagata, K., Nishitani, M., Matsuo, M., Kioka, N., Amachi, T. and Ueda, K. (2000) Nonequivalent nucleotide trapping in the two nucleotide binding folds of the human multidrug resistance protein MRP1. J. Biol. Chem. **275**, 17626–17630
25 Hou, Y. X., Cui, L., Riordan, J. R. and Chang, X. B. (2002) ATP binding to the first nucleotide-binding domain of multidrug resistance protein MRP1 increases binding and hydrolysis of ATP and trapping of ADP at the second domain. J. Biol. Chem. **277**, 5110–5119
26 Manciu, L., Chang, X. B., Buyse, F., Hou, Y. X., Gustot, A., Riordan, J. R. and Ruysschaert, J. M. (2003) Intermediate structural states involved in MRP1-mediated drug transport: role of glutathione. J. Biol. Chem. **278**, 3347–3356
27 Hou, Y. X., Riordan, J. R. and Chang, X. B. (2003) ATP binding, not hydrolysis, at the first nucleotide-binding domain of multidrug resistance-associated protein MRP1 enhances ADP · Vi trapping at the second domain. J. Biol. Chem. **278**, 3599–3605
28 Yang, R., Cui, L., Hou, Y. X., Riordan, J. R. and Chang, X. B. (2003) ATP binding to the first nucleotide binding domain of multidrug resistance-associated protein plays a regulatory role at low nucleotide concentration, whereas ATP hydrolysis at the second plays a dominant role in ATP-dependent leukotriene C_4 transport. J. Biol. Chem. **278**, 30764–30771
29 Bakos, É., Hegedüs, T., Holló, Z., Welker, E., Tusnády, G. E., Zaman, G. J. R., Flens, M. J., Váradi, A. and Sarkadi, B. (1996) Membrane topology and glycosylation of the human multidrug resistance-associated protein. J. Biol. Chem. **271**, 12322–12326
30 Müller, M., Bakos, É., Welker, E., Váradi, A., Germann, U. A., Gottesman, M. M., Morse, B. S., Roninson, I. B. and Sarkadi, B. (1996) Altered drug-stimulated ATPase activity in mutants of the human multidrug resistance protein. J. Biol. Chem. **271**, 1877–1883
31 Sarkadi, B., Price, E. M., Boucher, R. C., Germann, U. A. and Scarborough, G. A. (1992) Expression of the human multidrug resistance cDNA in insect cells generates a high activity drug-stimulated membrane ATPase. J. Biol. Chem. **267**, 4854–4858
32 Bakos, É., Evers, R., Sinkó, E., Váradi, A., Borst, P. and Sarkadi, B. (2000) Interactions of the human multidrug resistance proteins MRP1 and MRP2 with organic anions. Mol. Pharmacol. **57**, 760–768
33 Goodno, C. C. (1982) Myosin active-site trapping with vanadate ion. Methods Enzymol. **85**, 116–123
34 Bakos, É., Evers, R., Szakács, G., Tusnády, G. E., Welker, E., Szabó, K., de Haas, M., van Deemter, L., Borst, P., Váradi, A. and Sarkadi, B. (1998) Functional multidrug resistance protein (MRP1) lacking the N-terminal transmembrane domain. J. Biol. Chem. **273**, 32167–32175

35 Flens, M. J., Izquerido, M. A., Scheffer, G. L., Fritz, J. M., Meijer, C. J. L. M., Scheper, R. J. and Zaman, G. J. R. (1994) Immunochemical detection of the multidrug resistance-associated protein MRP in human multidrug-resistant tumor cells by monoclonal antibodies. Cancer Res. **54**, 4557–4563
36 Tusnády, G. E., Bakos, É., Váradi, A. and Sarkadi, B. (1997) Membrane topology distinguishes a subfamily of the ATP-binding cassette (ABC) transporters. FEBS Lett. **402**, 1–3
37 Holló, Z., Homolya, L., Hegedüs, T. and Sarkadi, B. (1996) Transport properties of the multidrug resistance-associated protein (MRP) in human tumour cells. FEBS Lett. **383**, 99–104
38 Rosenberg, M. F., Velarde, G., Ford, R. C., Martin, C., Berridge, G., Kerr, I. D., Callaghan, R., Schmidlin, A., Wooding, C., Linton, K. J. and Higgins, C. F. (2001) Repacking of the transmembrane domains of P-glycoprotein during the transport ATPase cycle. EMBO J. **20**, 5615–5625
39 Rosenberg, M. F., Kamis, A. B., Callaghan, R., Higgins, C. F. and Ford, R. C. (2003) Three-dimensional structures of the mammalian multidrug resistance P-glycoprotein demonstrate major conformational changes in the transmembrane domains upon nucleotide binding. J. Biol. Chem. **278**, 8294–8299
40 Chang, X. B., Hou, Y. X. and Riordan, J. R. (1997) ATPase activity of purified multidrug resistance-associated protein. J. Biol. Chem. **272**, 30962–30968

Received 21 October 2003/20 January 2004; accepted 3 February 2004
Published as BJ Immediate Publication 3 February 2004, DOI 10.1042/BJ20031607